Jour. of the KGS, Vol. 23, No. 3. March 2007, pp. 89~100

Elastic-plastic Micromechanics Modeling of Cross-anisotropic Granular Soils: II. Micromechanics Analysis

직교 이방적 사질토의 미시역학적 탄소성 모델링: II. 미시역학적 해석

Jung, Young-Hoon[1] 정 영 훈
Chung, Choong-Ki[2] 정 충 기

요 지

본 논문과 함께 제출한 논문에서는 미시역학 기반의 새로운 탄소성 모델의 정식화에 대해 설명하였다. 본 논문에서는 사질토 변형의 탄성 및 탄소성 거동을 미시역학에 근거하여 자세히 분석하였다. 모델에 필요한 변수 평가를 위한 과정을 제시하였다. 등방 및 삼축 압축 시험에서 나타난 사질토의 탄성 거동을 분석한 결과, 직교 이방 탄성계수의 응력 종속성은 미시적 수직 강성에서 나타난 수직 접촉력의 거듭제곱 함수 형태가 반영되어 나타나며, 삼축 압축 응력 상태에서는 조직 이방성의 변화가 응력 종속성에 영향을 미침을 알 수 있었다. 미시역학적 해석을 통해 소성 변형이 매우 낮은 변형률 수준에서도 발현되며, 변형 중 사질토 강성의 비선형적 감소는 접촉점에서의 접선 방향 소성 변형에 의해 나타남을 밝혔다.

Abstract

In the companion paper, we provided the novel elastic-plastic constitutive model based on the micromechanics theory. Herein, the elastic and elastic-plastic deformation of granular soils is meticulously analyzed. To guarantee high accuracy of the microscopic parameter, the systematic procedure to evaluate the parameters is provided. The analysis of the elastic response during the isotropic and triaxial compression shows that the stress-level dependency of cross-anisotropic elastic moduli is induced by the power relationship of the contact force in the normal contact stiffness, while the evolution of fabric anisotropy is more pronounced during triaxial compression. The micromechanical analysis indicates that the plastic strains are likely to occur at very small strains. The plastic deformation of tangential contacts has an important role in the reduction of soil stiffness during axial loading.

Keywords : Constitutive modeling, Elastic-plastic behavior, Granular soils, Micromechanics

1. Introduction

It is not questionable whether the behavior of the granular soil is the essential topic in the geotechnical area that a geotechnical professional should understand. The stress-strain behavior of granular soils has been understood within the notion of the elasticity as well as the elastic-plastic theory of the solid, which inevitably ignores the particulate feature of soils. Even though the existing framework of the finite element method, which is

1 Member, Post-doctoral fellow, Dept. of Civil and Env. Engrg., Northwestern Univ., 2145 Sheridan Rd. Rm. AG 50, Evanston, IL 60208, U.S.A., j-young-hoon@northwestern.edu, Corresponding Author
2 Member, Prof., School of Civil and Environment Engrg., Seoul National Univ., San 56-1, Shillim-dong, Kwanak-gu, Seoul 151-742, Korea

commonly employed in the geotechnical designs, is not likely to be abandoned without the presence of an ultimate theory to compensate for every single defect in the finite element method and its continuum-based constitutive model, it is quite necessary to expand our knowledge on the fundamental mechanisms of soil behavior, especially in the microscopic level of soil deformation.

The nonlinearity and anisotropy of the stress-strain responses in the granular soils are key features one needs to address to elevate the accuracy of the prediction in the geotechnical problems. Recalling the particulate nature of granular soils, one can suspect that both the nonlinearity and the anisotropy of soil deformation originate from the microscopic nonlinear anisotropic responses. In the companion paper, we derived the micromechanics-based elastic-plastic constitutive model, which includes a number of microscopic features the particles can possess. It was theoretically examined that the contacts in the particle assembly are nonlinearly deformed regardless of the elastic or elastic-plastic contacts.

In this paper, it will be shown that the macroscopic nonlinearity in the stress-strain responses relates to various microscopic features such as the nonlinear elastic and elastic-plastic contact stiffnesses. The elastic and plastic strains are decomposed into the strains induced by the normal and tangential contact deformations as well as the elastic and elastic-plastic contact deformation. The contributions of microscopic mechanisms are quantitatively examined, from which authors are to provide the theoretical basis to extend the understanding of the nonlinear cross-anisotropic deformation of the granular soils.

2. Summary of Micromechanics Formulations

The detailed derivation of the micromechanics-based elastic-plastic model was explained in the companion paper. Herein, the essential formulations in the model are summarized.

To characterize the heterogeneity of the contact distribution, the fabric tensor, F_{ij}, is introduced, given by

$$F_{ij} = \frac{Nd_g}{V}\int_{\Omega} n_i n_j E(\mathbf{n})d\Omega \tag{1}$$

where N is the number of contacts in an particle assembly, V is the total volume of the assembly, d_g is the mean diameter of particles within an assembly, n_i is the direction of the contact normal, $E(\mathbf{n})$ is the distribution function of the contact normals, and Ω is the unit sphere. The orientation distribution function, $E(\mathbf{n})$, is formulated based on the spherical harmonics with the symmetry of the vertical axis, as

$$E(\mathbf{n}) = E(\gamma) = \frac{3(1+a\cos 2\gamma)}{(3-a)} \tag{2}$$

where γ is the angle between the vertical axis in the global coordinate system and the contact normal, and a is the degree of fabric anisotropy.

Assuming the static hypothesis in defining the strains, the incremental compliance tensor, C_{ijkl}, is expressed by

$$\dot{\varepsilon}_{ij} = C_{ijkl}\dot{\sigma}_{kl} = \left[\rho_c \int_{\Omega} (n_m F_{lm}^{-1})(K_{ik})^{-1}(n_n F_{jn}^{-1})E(\mathbf{n})d\Omega\right]\dot{\sigma}_{kl} \tag{3}$$

where $\dot{\sigma}_{ij}$ and $\dot{\varepsilon}_{ij}$ are incremental stresses and strains, K_{ij} is the microscopic contact stiffness, F_{ij}^{-1} is the inverse of the fabric tensor, and ρ_c is the contact density relating to the void ratio, e, and co-ordination number, c_n, such that

$$\rho_c = \frac{N}{V} = \frac{3c_n}{\pi d_g^3(1+e)} = \frac{3(13.28-8e)}{\pi d_g^3(1+e)} \tag{4}$$

The microscopic contact stiffness, K_{ij}, in the global coordinate system is related to the normal contact stiffness, ${}^g k_n$, and the tangential contact stiffness, ${}^g k$, in the local coordinate system as

$$K_{ij} = {}^g k_n n_i n_j + {}^g k_r (s_i s_j + t_i t_j) \tag{5}$$

where n_i, s_i, and t_i denote the unit vectors corresponding the axes of the local coordinate system so that

As a general form, the elastic normal and tangential contact stiffnesses, ${}^g k_n^{el}$ and ${}^g k_r^{el}$, is expressed by

$${}^g k_n^{el} = c_n^{el}({}^g f_n / f_{ref})^{\alpha_n^{el}} \tag{6}$$

$${}^g k_r^{el} = c_r^{el}\,{}^g k_n^{el} \tag{7}$$

where f_{ref} is the normalizing constant (1 kN), c_n^{el} and c_r^{el} are the material constants relating to the geometry of the contact surface and the elastic modulus and Poisson's ratio of the particle, and ${}^{g}f_n$ is the normal contact force in the local coordinate system. The elastic-plastic normal contact stiffness, ${}^{g}k_n^{ep}$, which will be scaled up to the macroscopic elastic-plastic response, is defined by

$$ {}^{g}k_n^{ep} = c_n^{ep}({}^{g}f_n / f_{ref})^{\alpha_n^{ep}} = \frac{\theta(f_Y)^{1/\theta}}{\delta_Y}({}^{g}f_n)^{(\theta-1)/\theta} \tag{8} $$

where c_n^{ep} is the material constant, θ (=1.28) is the exponent which governs the power relationship of elastic-plastic contact behavior, and f_Y and δ_Y are the contact force and displacement initiating the yielding of the contact. The elastic-plastic tangential contact stiffenss, ${}^{g}k_r^{ep}$, is defined by

$$ {}^{g}k_r^{ep} = c_r^{ep}\,{}^{g}k_n^{ep}\left(1-\frac{{}^{g}f_r}{{}^{g}f_n\tan\phi_m}\right)^{\alpha_r^{ep}} \tag{9} $$

where c_r^{ep} is the material constant which is practically the same as c_r^{el}, ϕ_m is the friction angle of the particle, α_r^{ep} is the exponent defining the magnitude of nonlinearity induced by the frictional responses. To take the fabric evolution into account, the linear relationship between the degree of fabric anisotropy, a, and the macroscopic stress ratio, q/p, is employed, given by

$$ a = a_0 + a_1(q/p) \tag{10} $$

where a_0 is the degree of anisotropy in the isotropic stress condition, and a_1 is the slope of a for the increase of the stress ratio.

The approximate analytical solutions of cross-anisotropic elastic moduli in the isotropic stress condition are derived in terms of the micromechanical parameters, given by

$$ E_v^{el} = c_n^{el}c_r^{el}\left[\frac{7d_g^2\rho_c(5+a_0)^2}{5(3-a_0)\{14-2a_0+c_r^{el}(21+9a_0)\}}\right]\left[\frac{5(3-a_0)}{\rho_c d_g f_{ref}(5-3a_0)}\right]^{\alpha_n^{el}}(\sigma_0)^{\alpha_n^{el}} \tag{11a} $$

$$ E_h^{el} = c_n^{el}c_r^{el}\left[\frac{7d_g^2\rho_c(5-3a_0)^2}{5(3-a_0)\{14-6a_0+c_r^{el}(21-15a_0)\}}\right]\left[\frac{5(3-a_0)}{\rho_c d_g f_{ref}(5-3a_0)}\right]^{\alpha_n^{el}}(\sigma_0)^{\alpha_n^{el}} \tag{11b} $$

$$ G_{vh}^{el} = c_n^{el}c_r^{el}\left[\frac{7d_g^2\rho_c(5-3a_0)^2(5+a_0)^2}{10(5-a_0)(3-a_0)\left\{\begin{matrix}105-46a_0-23a_0^2\\+c_r^{el}(70-24a_0+2a_0^2)\end{matrix}\right\}}\right]\left[\frac{5(3-a_0)}{\rho_c d_g f_{ref}(5-3a_0)}\right]^{\alpha_n^{el}}(\sigma_0)^{\alpha_n^{el}} \tag{11c} $$

$$ G_{hh}^{el} = c_n^{el}c_r^{el}\left[\frac{7d_g^2\rho_c(5-3a_0)^2}{10(3-a_0)\{21-11a_0+c_r^{el}(14-10a_0)\}}\right]\left[\frac{5(3-a_0)}{\rho_c d_g f_{ref}(5-3a_0)}\right]^{\alpha_n^{el}}(\sigma_0)^{\alpha_n^{el}} \tag{11d} $$

where σ_0 is the macroscopic isotropic stress.

3. Identification of Micromechanics Parameters

The data obtained from a series of triaxial tests performed by Kuwano and Jardine (2002) were used to evaluate the model parameters. The soil was the Ham River sand with physical properties as summarized in Table 1. Complete details of the experiments are given by Kuwano (1999). To measure the elastic properties of the tested material, both small unload/reload cyclic tests and shear wave measurements using bender elements were conducted.

Basically, the model parameters involved with the elastic contact stiffness are determined by simply matching the approximate solutions of elastic moduli given in Eq. (11) to the empirical expressions of elastic moduli (1963) in the isotropic stress condition. The void ratio and mean diameter of particles were previously determined based on the physical properties for a specific sample. In the matching process, elastic Poisson's ratios are not considered particularly because the experimental measurement of the elastic Poisson's ratios is relatively inaccurate.

For the isotropic stress of σ_0, the empirical expressions of the cross-anisotropic elastic moduli are given by

Table 1. Physical properties of tested material (after Kuwano and Jardine, 2002)

Mineralogy	Specific gravity	Limit void ratio		Particle distribution		Particle shape
		e_{max}	e_{min}	D_{50}	U_c	
Quartz	2.66	0.849	0.547	0.27 mm	1.67	Sub-angular

U_c = Uniformity coefficient, D_{50} = Mean particle size, e_{max} = maximum void ratio, e_{min} = minimum void ratio. Maximum and minimum void ratios were determined following BS 1377.

$$E_v^{el} = A_v f(e) p_a^{-n_v} (\sigma_0)^{n_v} \quad (12a)$$

$$E_h^{el} = A_h f(e) p_a^{-n_h} (\sigma_0)^{n_h} \quad (12b)$$

$$G_{vh}^{el} = A_{vh} f(e) p_a^{-n_{vh}} (\sigma_0)^{n_{vh}} \quad (12c)$$

$$G_{hh}^{el} = A_{hh} f(e) p_a^{-n_{hh}} (\sigma_0)^{n_{hh}} \quad (12d)$$

where A_v, A_h, A_{vh}, and A_{hh} are the material constants, n_v, n_v, n_v, and n_v are the exponents indicating the stress-level dependence of experimental elastic moduli, and p_a is the atmospheric pressure (101.3 kPa), normalizing the macroscopic isotropic stress. The void ratio function, $f(e) = (2.17\text{-}e)^2/(1+e)$, used here is provided by Hardin and Richart (1963).

The value of α_n^{el} can be easily determined by comparing the exponents in Eqs. (11) and (12). The average of the experimentally determined values of n_v, n_h, n_{vh}, and n_{hh}, is taken as the value of α_n^{el}, while the values of A_v, A_h, A_{vh}, and A_{hh} are also adjusted to compensate for the change of the exponents in the empirical expressions. Table 2 summarizes the measured values of A and n, and their adjustments for the further use.

The degree of fabric anisotropy in the isotropic stress condition, a_0, and the proportional factor, c_r^{el}, can be determined by matching the moduli ratios, E_h/E_v and G_{hh}/G_{vh}, from the approximate solutions of Eq. (11) to those from the empirical expressions as:

$$\frac{E_h^{el}}{E_v^{el}} = \frac{A_h}{A_v} = \frac{(5-3a_0)^2}{(5+a_0)^2}\left[\frac{14-2a_0+c_r^{el}(21+9a_0)}{14-6a_0+c_r^{el}(21-15a_0)}\right] \quad (13a)$$

$$\frac{G_{hh}^{el}}{G_{vh}^{el}} = \frac{A_{hh}}{A_{vh}} = \frac{(5-a_0)}{(5+a_0)^2}\left[\frac{105-46a_0-23a_0^2+c_r^{el}(70-24a_0+2a_0^2)}{21-11a_0+c_r^{el}(14-10a_0)}\right] \quad (13b)$$

With the given values of A_h/A_v and A_{hh}/A_{vh}, the solution of Eqs. (13a) and (13b) yields the values of a_0 and c_r^{el}, as summarized in Table 3. As can be seen in Table 3, however, these estimations are unreasonable when considering the possible range of c_r^{el}, which should be positive and less than 1.0 based on the Mindlin's equation. To avoid such anomalous results, the values of a_0 are evaluated by employing either Eq. (13a) or Eq. (13b) with a fixed value of $c_r^{el} = 0.824$ based on the Poisson's ratio of 0.3 for the quartz. The remaining parameter, c_n^{el}, can be evaluated by substituting all the pre-determined values of α_n^{el}, c_r^{el}, a_0, e, and d_g into Eq. (11) and matching these to the empirical expressions in Eq. (12), thereby yielding four different values of c_n^{el} for each test. The average of four values is chosen as the representative value of c_n^{el}.

The sign of a_0 from Eq. (13a) is different from that from Eq. (13b), which is physically inadmissible in an identical sample. This contradictory result may come from the particular assumption to estimate the elastic moduli: Kuwano and Jardine (2002) assumed that the elastic properties obtained from small-cyclic triaxial tests are compatible with those from bender element tests to obtain a complete set of cross-anisotropic elastic moduli. As reported by Chaudhary et al. (2004) and Yimsiri and Soga (2002), such discrepancy in the value of a_0 was found in other experimental data but has not been clearly explained yet. Herein either set of parameters based on Eq. (13a) or (14b) is selectively adopted. For instance, the set of parameters based on Eq. (13a) is used to compute the Young's moduli such as E_v^{el} and E_h^{el}, while

Table 2. Material constants for empirical expressions of cross-anisotropic elastic stiffnesses (adjusted values are in parentheses)

Elastic Modulus	A (MPa)	Exponent			Relevant Expression (P_a =101.3kPa)
		a	b	$a+b$	
E_v^{el}	A_v = 204(204)	0.52(0.52)	-	0.52(0.52)	$E_v^{el} = A_v f(e)(\sigma_v / p_a)^{a_v}$
E_h^{el}	A_h = 174(176)	-	0.53(0.52)	0.53(0.52)	$E_h^{el} = A_h f(e)(\sigma_h / p_a)^{b_h}$
G_{vh}^{el}	A_{vh} = 72(72)	0.32(0.32)	0.20(0.20)	0.52(0.52)	$G_{vh}^{el} = A_{vh} f(e)\left(\frac{\sigma_v}{p_a}\right)^{a_{vh}}\left(\frac{\sigma_h}{p_a}\right)^{b_{vh}}$
G_{hh}^{el}	A_{hh} = 81(82)	-0.04(-0.03)	0.53(0.55)	0.50(0.52)	$G_{hh}^{el} = A_{hh} f(e)\left(\frac{\sigma_v}{p_a}\right)^{a_{hh}}\left(\frac{\sigma_h}{p_a}\right)^{b_{hh}}$

another set based on Eq. (13b) is chosen to compute the elastic shear moduli such as G_{vh}^{el} and G_{hh}^{el}.

If the contact force to initiate the elastic-plastic deformation of a single particle is f_Y, the magnitudes of elastic contact stiffness and elastic-plastic contact stiffness are approximately the same when $f_n = f_Y$:

$$C_n^{ep}(f_Y)^{\alpha_n^{ep}} = C_n^{el}(f_Y)^{\alpha_n^{el}} \quad \text{and} \quad C_n^{ep} = C_n^{el}(f_Y)^{\alpha_n^{el}-\alpha_n^{ep}} \tag{14}$$

In Eq. (14), the values of c_n^{el} and α_n^{el} were already evaluated. The value of α_n^{eP} is assumed to be 0.22 as described in the companion paper so that the determination of f_Y is important to find the value of C_n^{ep}. If the yielding is initiated in the conical contact, f_Y can be estimated by the following equation:

$$f_Y = \frac{\pi r_c^2}{8}\frac{(1-\nu_g)^2}{G_g^2}Y^3 \tag{15}$$

For the granular soils, the definite value of yield stress, Y, is difficult to find, because the yielding or failure point of brittle material is not well defined and affected by the size of specimen and the confining pressure. However, the yield stress can be estimated using the relation between Vickers diamond pyramid hardness parameter, H_V, and the yield stress, Y, (Johnson 1985), given by

$$H_V \approx 2.8Y \tag{16}$$

For quartz, with a hardness of about 10 GPa (Brace 1963), the value of Y is the order of 3 GPa. The approximate value of r_c can be obtained from the relation between the shape of particle and the 'roundness' parameter which is estimated by comparing the curvature of different surface features in the particle to the lowest curvature that can be assigned to the particle (e.g., the radius of the largest sphere that can be inscribed in the particle). For the 'sub-angular' particle, the value of r_c is about 3.4 ~ 4.7×10^{-2} mm (Jung 2004). For the selected material of quartz, with G_g = 29 GPa, ν_g = 0.31, Y = 3 GPa, and r_c = 3×10^{-2} mm, the value of f_Y is 5×10^{-6} kN. Using Eq. (14), the value of C_n^{ep} can be evaluated as summarized in Table 3. The parametric studies are needed to evaluate the remaining parameters, a_1 and α_r^{ep}.

Table 3. Summary of the evaluated parameters

Material parameters		Values	Note
Void ratio	e_0	0.658	initial void ratio
Mean diameter	d_g (mm)	0.27	D_{50}
Elastic contactstiffness	c_n^{el} (kN/m)	19775	using Eq. (13a); for E_v^{el} and E_h^{el}
		17599	using Eq. (13b); for G_{vh}^{el} and G_{hh}^{el}
	c_r^{el}	-0.982	using Eq. (13a) and (13b); not used
		0.824	$2(1-\nu_g)/(2-\nu_g)$ for ν_g = 0.3
	α_n^{el}	0.52	based on the experimental data
Elastic-plastic contact stiffnes	c_n^{ep} (kN/m)	513.6	$C_n^{ep} = C_n^{el}(f_Y)^{\alpha_n^{el}-\alpha_n^{ep}}$; f_Y = 5×10^{-6} kN for quartz
		451.7	
	α_n^{ep}	0.22	θ = 1.28
	c_r^{ep}	0.824	$c_r^{ep} = c_r^{el}$
	α_r^{ep}	3.0	based on the parametric study
	ϕ_m (deg)	26	referring to published data
Evolution of fabric anisotropy	a_0	-0.103	using Eq. (13a) and (13b); not used
		0.171	using Eq. (13a); for E_v^{el} and E_h^{el}
		-0.244	using Eq. (13b); for G_{vh}^{el} and G_{hh}^{el}
	a_1	0.34	based on the parametric study

4. Micromechanics Analysis of Granular Soils

4.1 Elastic Behavior

The main experimental features of macroscopic responses in granular soils are summarized as: (i) the elastic responses exhibit the cross-anisotropic elasticity, and (ii) the magnitude of each elastic modulus depends on the stress level in the form of the power function. These two features are manifested as the empirical correlations of the elastic moduli, thus the value of elastic modulus in any stress state can be estimated from the empirical expressions such as Eq. (12). From the viewpoint of the micromechanics theory, it is supposed that the cross-anisotropy of soil elasticity relates to the fabric tensor and the stress-level dependency of elastic moduli relates to the nonlinear contact stiffness depending on the level of contact forces, respectively.

The problem arises in the quantitative assessment of each role of two micro-mechanisms. In the previous section, except for a_1, the required parameters for the micromechanics analysis were precisely evaluated. Using these parameters, the elastic moduli are computed along two different stress paths—the isotropic compression and the triaxial compression, as shown in Fig. 1.

Fig. 2 compares the computed values of the Young's moduli and elastic shear moduli for the isotropic compression (IC) to the experimental data of each test. The value of a_1, which relates the variation of a to the stress ratio, is set to zero for the isotropic compression. As can be seen in Fig. 2 (a), the computed and measured data are practically identical, indicating that a certain degree of errors in the approximation of the closed-form solutions does not affect the reliability of prediction, partly due to relatively low degrees of fabric anisotropy. Moreover, this result confirms that the ignorance of the fabric evolution by setting a_1 to zero does not affect the accuracy of

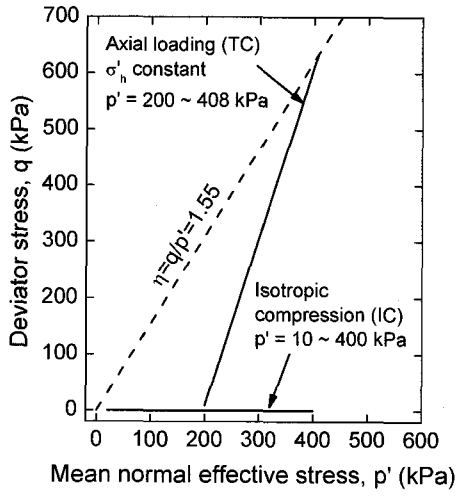

Fig. 1. Stress paths for the numerical simulation

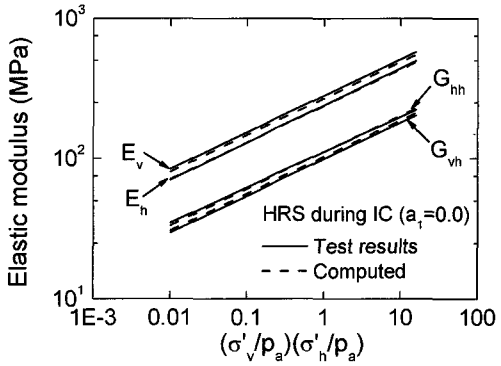

Fig. 2 (a) Variation of elastic moduli (for the constant a in the isotropic compression)

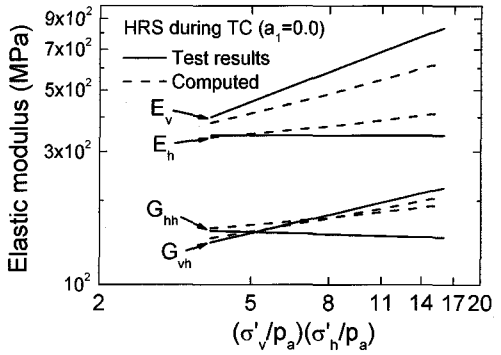

Fig. 2 (b) Variation of elastic moduli (for the constant a in the triaxial compression)

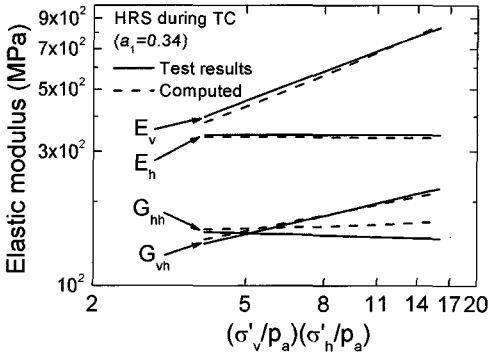

Fig. 2 (c) Variation of elastic moduli (for the varying a in the triaxial compression)

prediction. This also implies that the soil fabric remains constant when the samples are subject to the isotropic stress. In the isotropic stress condition, therefore, the stress-level dependency of cross-anisotropic elastic behavior is fully explained based on the nonlinear contact stiffness in the constant fabric condition. The exponent of the power function in the normal contact stiffness manifests itself as the exponent in the empirical expression of cross-anisotropic elastic modulus in the isotropic stress condition.

Fig. 2 (b) shows the computed and testing data during the triaxial compression (TC). In this case the value of a_1 is equal to zero, thus leading to the constant fabric condition as it was in the isotropic compression. As shown in Fig. 2 (b), even though the computed values of elastic moduli keep increasing during loading, the computed trend lines significantly differ from the experimental trend in elastic moduli. This discrepancy implies that in the anisotropic stress condition, the nonlinear contact stiffness at the constant fabric is not sufficient to explain the stress-level dependency of elastic moduli, and thus the remaining micromechanical feature—the evolution of fabric anisotropy—must be taken into account.

Within the framework of this research, the evolution of fabric anisotropy can be taken into account via a single parameter a_1 in Eq. (10). As noted previously, the value of a_1 implicitly includes the directional evolution of contact forces during loading. To choose a proper value of a_1, a parametric study is conducted. In the parametric study, the exponent of n in the empirical expression of test data is compared to the exponent of α obtained by the regression fitting on the computed elastic moduli of E_v^{el}, E_h^{el}, G_{vh}^{el}, and G_{hh}^{el} versus the applied stresses in the triaxial compression. The average of four different values of $|n - \alpha|$ for E_v^{el}, E_h^{el}, G_{vh}^{el}, and G_{hh}^{el} is taken to plot against the variation of a_1, as shown in Fig. 3. The results show that the value of $|n - \alpha|$ gradually decreases as a_1 increase, and minimized when a_1 = 0.34. Hence, the optimum expression to describe the evolution of fabric anisotropy for the triaxial compression, is given by

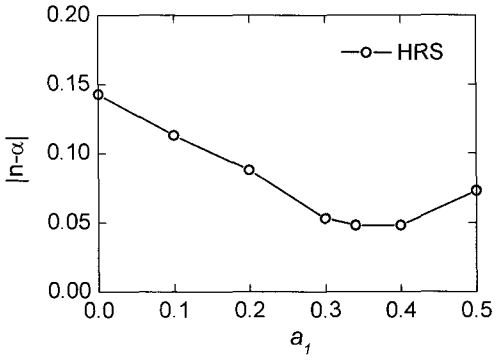

Fig. 3. Variation of $|n-\alpha|$ for the various values of a_1

$$a = a_0 + 0.34(q/p) \tag{17}$$

A similar research on the variation of a_1 via the discrete element method (Jung et al. 2006) also confirms that a simple linear relationship between a and q/p is valid for lower value of the stress ratio in the compression tests. Using the value of a from Eq. (17) for a given q/p, the elastic moduli are re-computed and compared to the experimental data in Fig. 2 (c). As can be seen in Fig. 2 (c), all the trends of computed elastic moduli match up with those of experimental trends.

The stress-level dependency of cross-anisotropic elastic moduli can be completely explained only if one can fully account for the evolution of fabric anisotropy in the anisotropic stress condition, together with the nonlinearity of the contact stiffness which is pronounced in the isotropic stress condition. The evolution of fabric anisotropy can quantitatively be expressed as the linear function of the stress ratio, q/p, at least for the triaxial compression, while the further calibration of Eq. (17) would be necessary for the general loading conditions. The numerical results show that as the stress ratio, q/p, changes, the state of fabric needs to be changed along with the applied anisotropic stresses to reproduce the experimental elastic response for the given stress condition. As mentioned previously, the evolution of fabric originates from the inelastic strains and particle rotations in the microscopic level so that the evolution equation of Eq. (17) indicates the magnitude of effect of the inelastic behavior on the elastic responses. To develop a complete micromechanics model aiming on the simulation of overall elastic-plastic stress-strain behavior

of granular soils, the change of fabric—loss and creation of contacts followed by the change of contact directions—should be taken into account in its formulation. The feasibility of such formulation on the fabric evolution could be examined based on the evolution equation such as Eq. (17), which is independently derived from the observation of experimental elastic responses.

4.2 Elastic-plastic Behavior

In the drained triaxial compression test (TC), the simulation results obtained from the micromechanical analysis with the elastic-plastic contact models were compared with the experimental data. During TC, the actual measurements related to the elastic-plastic behaviour are taken on the vertical (axial) stresses, the vertical (axial) strains and the horizontal (radial) strains. Thus, the physical quantities directly obtained from the measurements are the vertical Young's modulus, E_v^{ep}, and the Poisson's ratio, ν_{vh}^{ep}. The arbitrary assumptions are usually accompanied to obtain the other quantities such as E_h^{ep}, ν_{hh}^{ep} and ν_{hv}^{ep}. Herein, the quantitative comparisons between the computed and the measured data will be limited to E_v^{el} and ν_{vh}^{ep}.

In the micromechanics analysis, it is assumed that the degree of fabric anisotropy continuously changes with the stress ratio. The inclination of the linear a - η curve, a_1 is set to 0.34 which gives the best-fitting results for the stress-level-dependent behavior of the elastic moduli. The initial value of the degree of fabric anisotropy, a_0, however, is still uncertain because the inconsistency in the value of a_0 is not resolved. Thus, the possible values of a_0 between 0.171 from Eq. (13a) and -0.224 from Eq. (13b) are applied and the different responses of elastic-plastic modulus, E_v^{ep}, are examined. In addition, as discussed in the previous section, the parameter α_r^{ep} for the tangential contact stiffness is not defined. Herein, the value of α_r^{ep} is set to 3.0 based on the parametric study conducted by Jung (2004). Fig. 4 summarizes the results of the simulation for $\alpha_r^{ep} = 3.0$. It is noted that the scattering of measured tangent modulus in Fig. 4 (a) is inevitable due to the limitation of measurement of the stresses and strains at small strains. The scatters of tangent modulus do not appear in the variation of secant modulus as shown in Fig. 4 (b).

The numerical results in Fig. 4 provide useful information on the elastic-plastic behavior during the axial compression. Fig. 5 shows the stress-strain curves in the vertical direction for various strain levels. The numerical findings for the elastic-plastic behavior during triaxial compression are:

(1) The plastic strains are likely to occur even at very small strains. The linear response of the stress-strain curve at very small strains does not indicate the pure elastic response of soils. Combination of the increasing elastic modulus with the increasing vertical stress and the plastic strains degrading the slope of stress-strain curve produces the apparent linearity in the initial part of the stress-strain curve.

(2) At very small strains, the effect of plastic straining on the degradation of elastic-plastic modulus is minimized when the initial state of soil is under the isotropic

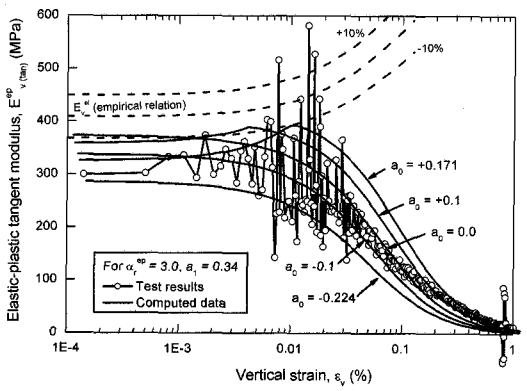

Fig. 4 (a) Variation of E_v^{ep} with the different a_0 during triaxial compression (tangent modulus)

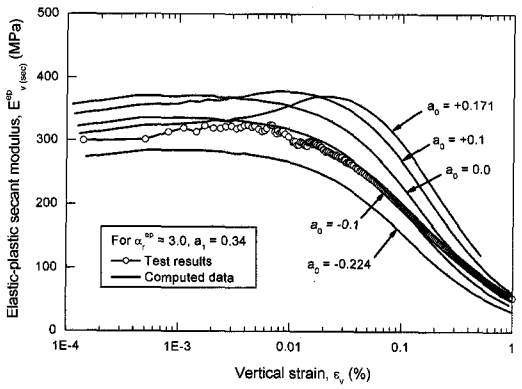

Fig. 4 (b) Variation of E_v^{ep} with the different a_0 during triaxial compression (secant modulus)

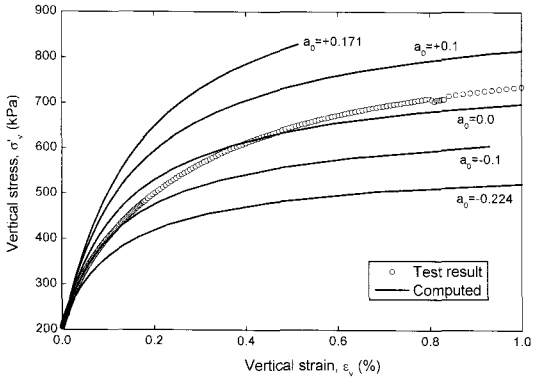

Fig. 5 (a) Stress-strain curves in the vertical direction (up to 1%)

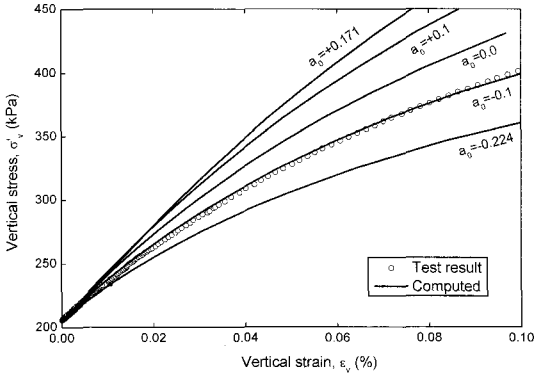

Fig. 5 (b) Stress-strain curves in the vertical direction (up to 0.1%)

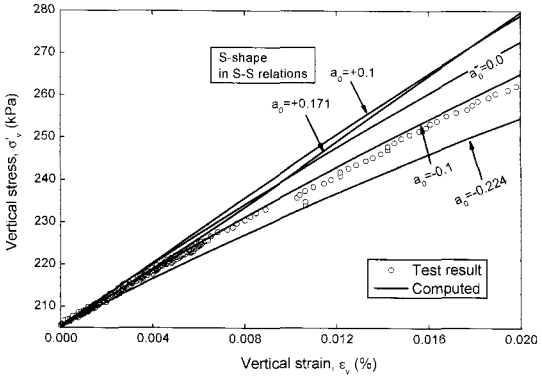

Fig. 5 (c) Stress-strain curves in the vertical direction (up to 0.02%)

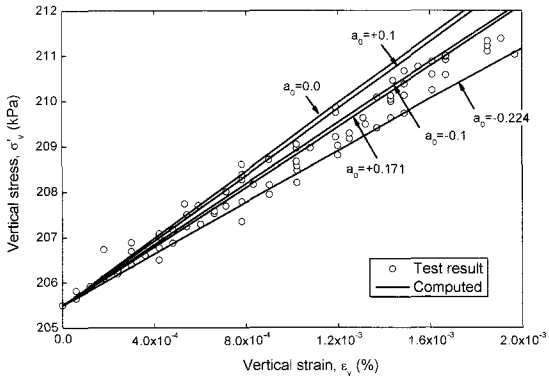

Fig. 5 (d) Stress-strain curves in the vertical direction (up to 0.002%)

fabric condition (i.e. $a_0 = 0.0$). The larger a_0 deviates from the isotropic value of 0.0, the larger decrease of initial modulus takes place.

(3) When $a_0 > 0$, the increasing pattern of E_v^{ep} appears at small strains. Due to the increasing modulus, the apparent linear range in the stress-strain relations increased up to about $\varepsilon_v = 0.01\%$ (see Fig. 5(c)). When a_0 is less than or equal to zero, however, E_v^{ep} continuously decreased with the axial strains. If the increase of E_v^{ep} can be regarded as the linear elastic response, the size of elastic region increases as the value of a_0 increases.

(4) For a specific value of α_r^{ep}, the magnitude of E_v^{ep} for the higher value of a_0 is larger than that for the lower value of a_0 after the axial strain exceed 0.01%.

It is interesting that the values of E_v^{ep} increase in the small strain range and the corresponding 'S-shaped' stress-strain relationship appears when $a_0 > 0.0$. The similar pattern of increasing E_v^{ep} can be found in the other experimental results reported by Kohata et al. (1997). They observed that the increasing E_v^{ep} and the 'S-shaped' stress-strain relationships in the cyclic pre-strained specimens in which the larger number of cycles was applied to the specimen, the higher increase of E_v^{ep} took place. This experimental phenomena are very similar to the numerical results for $a_0 > 0$ in Figs. 4 and 5. In terms of micromechanics, it can be thought that the process of the cyclic pre-straining increases the number of contacts in the vertical (axial) direction. The maximum value of E_v^{ep} for $a_0 = +0.171$ is larger than that for $a_0 = +0.1$. Based on the above discussion, one can conclude that the increase of E_v^{ep} during compression is the distinctive feature of the stress-strain response for the initial fabric condition with $a_0 > 0$. It is noted that the experimental data of stress-strain curves in Fig. 5 does not show the particular 'S-shaped' pattern during compression. This may imply that the initial state of fabric anisotropy is close to the condition with $a_0 < 0$. There is a possibility that $a_0 < 0.0$ obtained from Eq. (13b) represents the real state of the initial condition of specimen more closely.

Fig. 6 shows the contribution of elastic and plastic strains to the total strains in the vertical direction. For

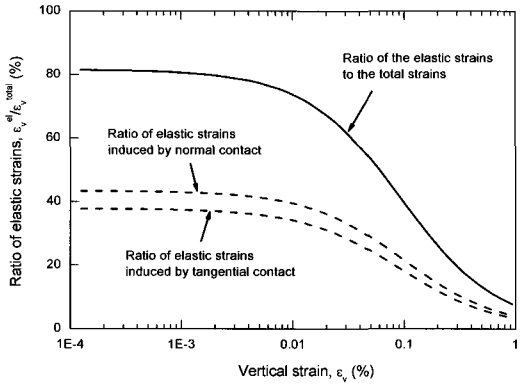

Fig. 6 (a) Strains developed in the vertical direction (elastic and total strains)

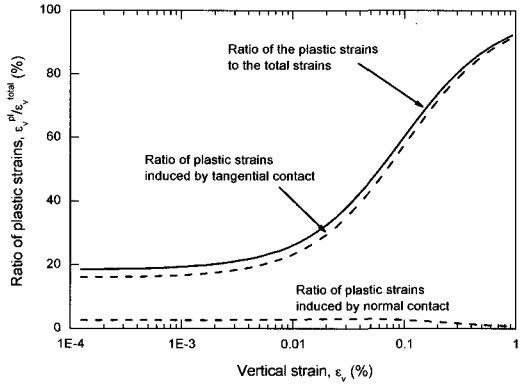

Fig. 6 (b) Strains developed in the vertical direction (plastic and total strains)

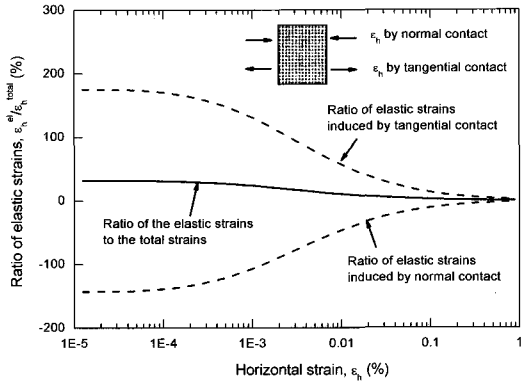

Fig. 7 (a) Strains developed in the horizontal direction (elastic and total strains)

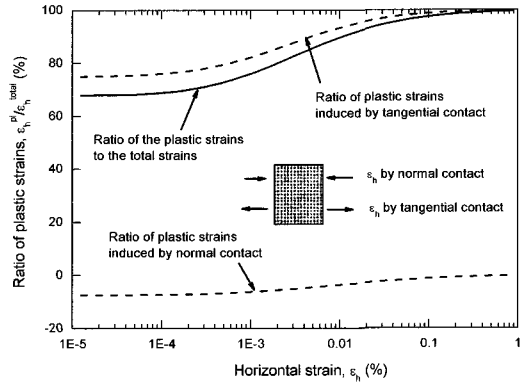

Fig. 7 (b) Strains developed in the horizontal direction (plastic and total strains)

convenience, the numerical results for a_0 = -0.1, which closely matched the experimental relationship between E_v^{ep} and ε_v, are analyzed. The strains are decomposed into the components induced by normal and tangential contacts displacements to investigate the effect of contact stiffnesses on the overall behavior of elastic-plastic straining.

Fig. 6 shows that the contribution of elastic strains, which initially occupies about 80% of total strains, continuously reduces during axial compression. The elastic strains induced by the tangential contacts have a considerable portion of total elastic strains compared with those induced by the normal contacts. However, in case of the plastic strains, the different pattern of the contribution of strains induced by the normal and the tangential contacts takes place. The ratio of plastic strains induced by the normal contacts is very small in the overall strain range. The plastic strains induced by the tangential contacts occupy most of the plastic strains. Thus, one may conclude that the plastic strains, which reduce the stiffness in the vertical direction, are mainly controlled by the properties of tangential contact stiffness. The contributions of elastic and plastic strains in the total horizontal strains, however, are quite different from those in the vertical strains. Fig. 7 shows the ratio of elastic and plastic strains to the total strains in the horizontal direction. The differences between the responses in the vertical and horizontal strains can be summarized as follows:

(1) While both of the elastic strains induced by the normal contact and the elastic strains induced by the tangential contact are in compression in the vertical direction, the direction of horizontal strains induced by the normal contact are opposite to that by the tangential contact. The elastic strains induced by the normal contacts are developed in the compression side of the horizontal direction, but the elastic strains induced by the tangential contacts are in the extension. The same pattern of the plastic straining takes place.

(2) In the horizontal strains, the ratio of elastic strain to

total strain is only about 20~40% even at the very small strains. The horizontal strains induced by the plastic deformation or slippage induced by the tangential contacts occupy most of the horizontal strains during axial loading. Similar to the pattern of the vertical strains, the plastic strains induced by the normal contacts occupy the small portion of the total plastic strains in the overall horizontal strains.

The cross-anisotropic Poisson's ratios are also affected by the magnitude of the horizontal strains. Fig. 8 shows the variation of cross-anisotropic Poisson's ratios during triaxial compression. In the triaxial compression, the value of $\nu_{vh}^{ep} = -\delta\varepsilon_h^{ep} / \delta\varepsilon_v^{ep}$ can be measured during test. The pattern of variation in the computed values of ν_{vh}^{ep} is similar to that in the test data. For the elastic-plastic values of Poisson's ratios, ν_{vh}^{ep} is generally higher than ν_{hv}^{ep} and ν_{hh}^{ep} because the magnitude of ν_{vh}^{ep} is significantly affected by the magnitude of ε_h^{ep}. In the overall strains, ν_{hh}^{ep} ranging from 0.1 to 0.35 is lower than the other two Poisson's ratios. It should be noted that the elastic Poisson's ratios are nearly zero and do not exceed 0.1. The value of ν_{vh}^{ep} increases with the axial strains from the values close to ν_{vh}^{el} to the values of $\nu_{vh}^{pl} = -\delta\varepsilon_h^{pl} / \delta\varepsilon_v^{pl}$. Hayano and Tatsuoka (1997) reported the similar behavior of ν_{vh}^{el}, ν_{vh}^{pl} and ν_{vh}^{ep} from a drained triaxial compression test, from which it may be considered that values of ν_{vh}^{ep} exceeding 0.1 at the very small strains in the drained compression test indicate the generation of the plastic strains primarily induced by tangential contacts.

The above analysis results ascribed the overall degradation of soil stiffness mainly to the plastic strains induced by the tangential contacts. However, the shear failure of particulate materials after dilation seems not to be massive as much as the micromechanics model predicts. Even before failure, the groups of particles, in general, move together in 'wedges'. Eventually, neighboring wedges become kinematically locked, they shear, and a new subsystem of wedges is formed. In many cases, deformations continue localizing in narrow shear bands. Once such mechanism is formed, the blocks bound by the slip plane move as rigid bodies and deformation localizes within the slip planes producing progressive failure. The internal energy exerted on the tangential contacts at the early stage of shearing is transferred to the localized slip plane generating two sliding 'wedges' at the large strains. The micromechanics approach with homogenization technique adopted in this study cannot simulate such a localization of the particulate structure experiencing large strains. Consequently, there is a possibility to underestimate the stiffnesses of soils subjected to the large deviator stress. The plastic strain in every single contact in the homogenization technique leads to the excessive volumetric expansion at the early stage of shearing. Fig. 9 compares the volumetric strains in the test data and the numerical results in the large strain range. While the computed stress-strain relationship shows the good agreement before the deviator stress reaches a stress point at the onset of marked dilation, significant discrepancy between the test and computed data appears after the apparent dilation takes place. Different method such as the bifurcation

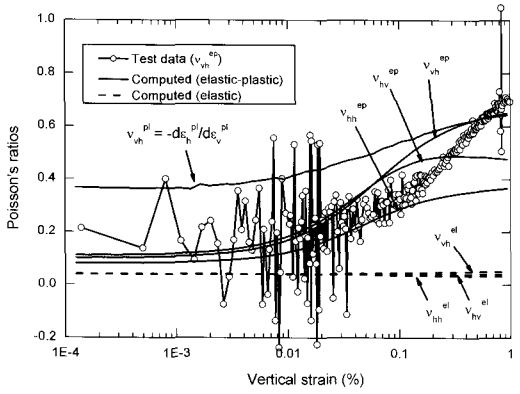

Fig. 8. Cross-anisotropic Poisson's ratios during triaxial compression

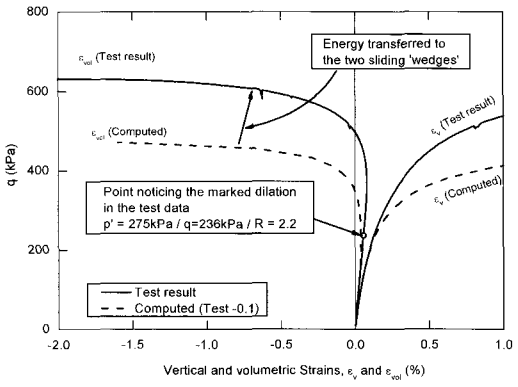

Fig. 9. Vertical and volumetric strains during shearing in test data and simulations

analysis would be useful to predict the stress-strain behavior after a particulate material shows the dilation.

5. Conclusions

In terms of the micromechanics theory, the elastic and elastic-plastic responses of deformation of granular soils are meticulously analyzed. To guarantee the high accuracy of the microscopic parameter, the systematic procedure to evaluate the parameters is provided. The parameters involved with the elastic contact stiffness are mainly evaluated by the direct comparison between the empirical expression of cross-anisotropic elastic moduli and the micromechanics-based analytical solutions. The parameters to formulate the elastic-plastic contact stiffness are determined based on the published experimental data for the metallic materials as well as the material references.

The analysis of the elastic response during the isotropic and triaxial compression shows that the stress-level dependency of cross-anisotropic elastic moduli is induced by the power relationship of the contact force in the normal contact stiffness, while the evolution of fabric anisotropy is more pronounced during triaxial compression. The evolution of fabric anisotropy is quantitatively evaluated by observing the difference between the experimental data and the micromechanical predictions.

In the light of the micromechanics theory, the elastic-plastic responses of soil deformation are thoroughly scrutinized. The micromechanical analysis indicates that the plastic strains are likely to occur at the very small strains. The linear response of the stress-strain curve at the very small strains does not represent the pure elastic response of soils. The combination of the stress-level-dependent elastic modulus and the plastic straining generates the apparent linearity in the initial part of the stress-strain curve. The magnitude of the elastic strains induced by the tangential contacts is comparable to the strains induced by the normal contacts. However, in the case of the plastic strains, the pattern of contribution between the normal and the tangential contacts is different from the elastic case. The ratio of plastic strains induced by the normal contacts to the total plastic strains is very small in the overall strain range. The plastic strains induced by the tangential contacts occupy most of the plastic strains. The plastic deformation of tangential contacts has an important role in the reduction of soil stiffness during axial loading.

Acknowledgements

Financial support for this work was provided by Korea Research Foundation Grant No. KRF-2005-214-D00166. The support of Engineering Research Institute at Seoul National University is greatly appreciated.

References

1. Brace, W. F. (1963), "Behavior of quartz during indentation", *Journal of geology*, 71(5), 581-595.
2. Chaudhary, S. K., Kuwano, J., and Hayano, Y. (2004), "Measurement of quasi-elastic stiffness parameters of dense toyoura sand in hollow cylinder apparatus and triaxial apparatus with bender elements", *Geotechnical Testing Journal*, 27(1), 23-35.
3. Hardin, B. O., and Richart, F. E. J. (1963), "Elastic wave velocities in granular soils", *Journal of Soil Mechanics and Foundation Engineering, ASCE*, 89(SM1), 33-65.
4. Johnson, K. L. (1985), *Contact mechanics*, Cambridge University Press, Cambridge.
5. Jung, Y.-H., Lee, J.-H., and Chung, C.-K. (2006), "Evolution of Fabric Anisotropy in Granular Soils under Triaxial Loadings", *Proc. Geocongress 2006*, Atlanta, Georgia.
6. Jung, Y. H. (2004), "Modeling of nonlinear anisotropic deformation of granular soils in pre-failure condition by numerical approach", Seoul National University, Seoul, Korea.
7. Kohata, Y., Tatsuoka, F., Wang, L., Jiang, G. L., Hoque, E., and Kodaka, T. (1997), "Modelling the non-linear deformation properties of stiff geomaterials", *Geotechnique*, 47(3), 563-580.
8. Kuwano, R. (1999), "The stiffness and yielding anisotropy of sand", Ph.D. thesis, Imperial college, University of London, London.
9. Kuwano, R., and Jardine, R. J. (2002), "On the applicability of cross-anisotropic elasticity to granular materials at very small strains", *Geotechnique*, 52(10), 727-749.
10. Yimsiri, S., and Soga, K. (2002), "Application of micromechanics model to study anisotropy of soils at small strains", *Soils and Foundations*, 42(5), 15-26.

(received on Jan. 12, 2007, accepted on Mar. 26, 2007)